Journal of Sound and Vibration 329 (2010) 4785–4796

Contents lists available at ScienceDirect

Journal of Sound and Vibration

journal homepage: www.elsevier.com/locate/jsvi

Nodal line optimization and its application to violin top plate design

Yonggyun Yu [a], In Gwun Jang [b], In Kyum Kim [c], Byung Man Kwak [a,*]

[a] Department of Mechanical Engineering, Korea Advanced Institute of Science and Technology, Guseong-dong, Yuseong-gu, 305-701 Daejeon, Seoul, Republic of Korea
[b] Department of Ocean Systems Engineering, Korea Advanced Institute of Science and Technology, 305-701 Daejeon, Republic of Korea
[c] Electrotechnology R&D Center, LS Industrial Systems, 361-720 Cheongju, Chungcheongbuk-do, Republic of Korea

ARTICLE INFO

Article history:
Received 8 March 2010
Received in revised form
12 May 2010
Accepted 23 May 2010
Handling Editor: L.G. Tham
Available online 11 June 2010

ABSTRACT

In the literature, most problems of structural vibration have been formulated to adjust a specific natural frequency: for example, to maximize the first natural frequency. In musical instruments like a violin; however, mode shapes are equally important because they are related to sound quality in the way that natural frequencies are related to the octave. The shapes of nodal lines, which represent the natural mode shapes, are generally known to have a unique feature for good violins. Among the few studies on mode shape optimization, one typical study addresses the optimization of nodal point location for reducing vibration in a one-dimensional beam structure. However, nodal line optimization, which is required in violin plate design, has not yet been considered. In this paper, the central idea of controlling the shape of the nodal lines is proposed and then applied to violin top plate design. Finite element model for a violin top plate was constructed using shell elements. Then, optimization was performed to minimize the square sum of the displacement of selected nodes located along the target nodal lines by varying the thicknesses of the top plate. We conducted nodal line optimization for the second and the fifth modes together at the same time, and the results showed that the nodal lines obtained match well with the target nodal lines. The information on plate thickness distribution from nodal line optimization would be valuable for tailored trimming of a violin top plate for the given performances.

1. Introduction

When we perform music, the body of a musical instrument vibrates with the stroke of a hammer, the friction of a bow, or the turbulent flow of a stream of breath. The vibration of an instrument's body excites the air surrounding the body, generating vibration in the air with the same frequency. This vibration propagates through the air, generating a sound field. The sound spectrum radiated by musical instruments consists of the superposition of a number of partials. Every partial is characterized by its frequency, pressure strength and its decay rate. Such sound-related parameters are affected by eigenfrequencies and corresponding eigenmodes.

The current form of the violin was developed in the early eighteenth century based on 300 years of design experience. Violin craftsmen have intuitively tuned nodal lines, which are determined by natural frequencies and the mode shapes of a violin top plate, to those they desire. There have been various trends in the thickness distribution and arching of violin plates according to the nation or school where the instruments were produced. Although the violin was designed in a

* Corresponding author. Tel.: +82 42 350 3011; fax: +82 42 350 3210.
E-mail addresses: yonggyunyu@kaist.ac.kr (Y. Yu), jangin0407@gmail.com (I.G. Jang), ikkim@lsis.biz (I.K. Kim), bmkwak@kaist.ac.kr (B.M. Kwak).

0022-460X/$ - see front matter © 2010 Elsevier Ltd. All rights reserved.
doi:10.1016/j.jsv.2010.05.022

non-scientific manner, many engineers and scientists are still attempting to discover the secrets of Old Italian violins that are currently recognized to have the best sound quality. In the findings of one such study, it was reported that well designed violins have low eigenfrequencies within a specific range and that their eigenmodes have a specific shape of nodal lines.

Mode shapes (or the shape of nodal lines) and eigenfrequencies significantly affect sound parameters such as radiation efficiency and quality factor [1,2]. From this viewpoint of sound engineering, the shapes of nodal lines of a violin top plate have been inspected for various materials [3]. Actual behavior of an assembled violin would be different from that of a free violin top plate due to different boundary conditions and interactions with other components. Before assembling components, however, each component (mostly violin top and back plate) should be tuned separately first. The changes in the vibration characteristics that occur with changes to the thickness of a violin top plate have also been investigated [4]. The development of the nodal lines from a blank (base wood) to a finished violin top plate was investigated by Jansson et al. [2,5]. Starting with a blank, they found two nodal lines forming a cross for the first resonance. This nodal cross remained through all following adjustments. The second resonance initially had two horizontal nodal lines, but changed to typical nodal lines for a violin top plate that was arched and 8 mm thick. While varying the plate thickness between 4 and 5 mm, the fifth violin plate resonance, the ring mode, was found; this mode is known to be the most important and sensitive to thickness distribution. The aforementioned findings can actually improve the current violin design with the aid of state-of-the-art engineering analysis.

In most optimization problems related with vibration or sound, natural frequencies have often been considered more important than mode shapes. Specifically, maximization of a specific natural frequency is one of the most frequently used optimization formulations in the field [6,7]. Tinnsten and Carlsson [8,9] have performed the frequency optimizations of a violin plate with respect to various structural design variables, such as shell thickness, arching, material parameters, etc. However, the literature to date has rarely focused on mode shape optimization. Pritchard et al. [10] calculated the sensitivities of nodal point location for reducing the vibration of a one-dimensional simplified structure with beam and lumped mass, and Lai et al. [11] similarly conducted optimization to obtain the desired mode shape of a simple one-dimensional bar. Inzarulfaisham and Azegami [12] performed a shape optimization by using a traction method in order to obtain the targeted eigenvector and then minimized the vibration by applying a geometric boundary condition to several nodes in a chassis-like frame [13]. In topology optimization [14–17], Maeda et al. [18] proposed a new method for designing vibrating structures that targets desired eigenfrequencies and eigenmode shapes. In the aforementioned approaches, however, the solution for the adjoint equation (i.e., adjoint mode) is approximated as a linear combination of eigenmodes in the modal coordinate system, which requires a finite number of eigenmodes for accurate sensitivity calculation. Computational burden also usually increases as the number of target nodes increases. Therefore, it is not easy to apply these optimization techniques to complex, practical three-dimensional problems with a large number of design variables.

In this paper, we propose an efficient calculation for eigenvector sensitivities based on the adjoint equation with approximated stiffness and mass matrices, and element shape function representation. By adopting topology optimization techniques, we use a single design variable per finite element (element thickness in detail), which results in a high degree of flexibility in shape variation of the nodal line. These new features, for the first time to our knowledge, enable us to handle a violin top plate with complicated three-dimensional geometry for nodal line optimization, compared with the simple one- or two-dimensional cases in the literature.

We first introduced the basic idea of a nodal line optimization for violin design (Section 2.1) and then calculated the corresponding sensitivities for a gradient-based optimization algorithm with the aid of an approximated element stiffness matrix (Sections 2.2 and 2.3). By applying the proposed method and adjusting the thickness of a violin top plate (Sections 2.4 and 2.5), we successfully performed an optimization for the nodal lines of a violin top plate (Section 3). We concluded this paper by showing a direction of our further work.

2. Nodal line optimization

2.1. Concept of nodal line optimization

Depending on the eigenfrequencies, a structure vibrates with specific vibrating modes, where both zero and maximum amplitudes exist. In acoustics, a point with zero amplitude is called a node, and one with maximum amplitude is called an anti-node. A line that is composed of a set of nodes is called a nodal line. The shape of nodal lines is used to define the vibration features of a structure and has been commonly applied to the design of musical instruments

Fig. 1 shows the basic concept of nodal line optimization. In Fig. 1, small circles represent target nodes and dotted lines show the current nodal lines. By adjusting the thickness of each element, we tune the initial nodal lines in Fig. 1(a) to the desired lines in Fig. 1(b). As the number of nodes increases, we can fine-tune the nodal lines.

The eigenvalue problem in the form of finite element analysis is expressed as

$$\mathbf{K}\boldsymbol{\Phi}_j = \lambda_j \mathbf{M}\boldsymbol{\Phi}_j \quad \text{with} \quad \boldsymbol{\Phi}_j^{\mathrm{T}}\mathbf{M}\boldsymbol{\Phi}_j = 1 \tag{1}$$

where $\mathbf{K}$ denotes the stiffness matrix of a structure, $\mathbf{M}$ the mass matrix, $\boldsymbol{\Phi}_j$ the jth eigenvector, and λ_j the jth eigenvalue.

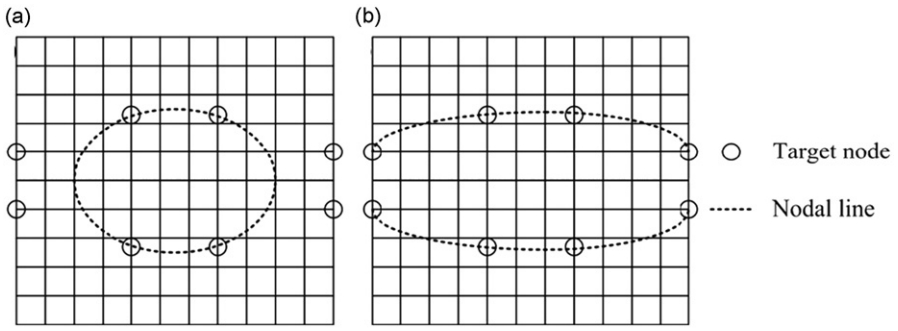

Fig. 1. Concept of nodal line optimization: (a) before optimization and (b) after optimization.

The nodal line, L, along which a vertical component of an eigenvector becomes zero, can be formulated as

$$L=\{\mathbf{x}|w_j(\mathbf{x})=\mathbf{N}\boldsymbol{\Phi}_j^i\cdot\mathbf{n}(\mathbf{x})=\mathbf{N}\mathbf{T}_i\boldsymbol{\Phi}_j\cdot\mathbf{n}(\mathbf{x})=0 \quad \text{for } \forall i\} \tag{2}$$

where $w_j(\mathbf{x})$ denotes the component of the jth eigenvector normal to a local tangential plane at $\mathbf{x}$, $\mathbf{N}$ the shape function matrix, $\boldsymbol{\Phi}_j^i$ the eigenvector of $\boldsymbol{\Phi}_j$ for the ith element to which $\mathbf{x}$ belongs, $\mathbf{T}_i$ the transformation matrix for the ith element, and $\mathbf{n}(\mathbf{x})$ a normal vector at $\mathbf{x}$ in $(x,y,z,\theta_x,\theta_z,\theta_y)$. Here, the shape function matrix, $\mathbf{N}$, is expressed with each shape fuction N_i where the corresponding degree of freedom (dof) has a unit value while the other dof is zero as in

$$\mathbf{N}=\begin{bmatrix} N_1 & 0 & 0 & 0 & 0 & 0 & N_2 & 0 & \cdots \\ 0 & N_1 & 0 & 0 & 0 & 0 & 0 & N_2 & \cdots \\ 0 & 0 & N_1 & 0 & 0 & 0 & 0 & 0 & \cdots \\ 0 & 0 & 0 & N_1 & 0 & 0 & 0 & 0 & \cdots \\ 0 & 0 & 0 & 0 & N_1 & 0 & 0 & 0 & \cdots \\ 0 & 0 & 0 & 0 & 0 & N_1 & 0 & 0 & \cdots \end{bmatrix} \tag{3}$$

Then, in order to pass the target node at $\mathbf{x}_i$, the nodal line, L, should satisfy

$$w_j(\mathbf{x}_i)=0 \tag{4}$$

For nodal line optimization, we first need to quantify the difference between the targeted and the current nodal lines. We define the error of the current nodal lines from the targeted ones for the jth mode as

$$\begin{aligned} E_j &= \sum_{i=1}^{n_n}(w_j(\mathbf{x}_i))^2 \\ &= \sum_{i=1}^{n_n}(\mathbf{N}\mathbf{T}_i\boldsymbol{\Phi}_j\cdot\mathbf{n}(\mathbf{x}_i))^2 \\ &= \sum_{i=1}^{n_n}(\mathbf{n}(\mathbf{x}_i)^{\mathrm{T}}\mathbf{N}\mathbf{T}_i\boldsymbol{\Phi}_j)^2 \end{aligned} \tag{5}$$

where n_n represents the number of target nodes. Here, for simplicity, we set the same subscription i for both target nodes and elements. If E_j=0, then a nodal line passes all target nodes perfectly.

2.2. Sensitivity analysis of nodal line optimization

Consider the general response function of an eigenproblem represented in terms of eigenvalues λ_j, eigenvectors $\boldsymbol{\Phi}_j$ and a design variable vector $\mathbf{b}$ as follows:

$$g=g(\lambda_j,\boldsymbol{\Phi}_j,\mathbf{b}) \tag{6}$$

It is assumed that the response function whose sensitivity is desired is continuous and differentiable with respect to its arguments. For the adjoint variable method [19,20], the Lagrangian function is defined by adding state equations to the response function as follows:

$$L=g(\lambda_j,\boldsymbol{\Phi}_j,\mathbf{b})+\mathbf{z}^{\mathrm{T}}(\mathbf{K}-\lambda_j\mathbf{M})\boldsymbol{\Phi}_j+y(\tfrac{1}{2}-\tfrac{1}{2}\boldsymbol{\Phi}_j^{\mathrm{T}}\mathbf{M}\boldsymbol{\Phi}_j) \tag{7}$$

where y and $\mathbf{z}$ are adjoint variables (or so-called Lagrange multipliers) for eigenvalues and eigenvectors, respectively. The adjoint variables y and $\mathbf{z}$ are determined such that the Lagrangian function L in Eq. (7) is stationary with respect to the

variations of the primary state variables; i.e.

$$\frac{\partial L}{\partial \lambda_j} = \frac{\partial g}{\partial \lambda_j} - \mathbf{z}^{\mathrm{T}}\mathbf{M}\boldsymbol{\Phi}_j = 0$$
$$\frac{\partial L}{\partial \boldsymbol{\Phi}_j} = \frac{\partial g}{\partial \boldsymbol{\Phi}_j} + (\mathbf{z}^{\mathrm{T}}(\mathbf{K}-\lambda_j\mathbf{M}))^{\mathrm{T}} - y(\boldsymbol{\Phi}_j^{\mathrm{T}}\mathbf{M})^{\mathrm{T}} = \mathbf{0} \tag{8}$$

By using the symmetry of $\mathbf{K}$ and $\mathbf{M}$,

$$\frac{\partial g}{\partial \lambda_j} - \boldsymbol{\Phi}_j^{\mathrm{T}}\mathbf{M}\mathbf{z} = 0$$
$$\frac{\partial g}{\partial \boldsymbol{\Phi}_j} + (\mathbf{K}-\lambda_j\mathbf{M})\mathbf{z} - y\mathbf{M}\boldsymbol{\Phi}_j = \mathbf{0} \tag{9}$$

Then, the adjoint equation is obtained as follows:

$$\begin{bmatrix} \mathbf{K}-\lambda_j\mathbf{M} & -\mathbf{M}\boldsymbol{\Phi}_j \\ -\boldsymbol{\Phi}_j^{\mathrm{T}}\mathbf{M} & 0 \end{bmatrix} \begin{bmatrix} \mathbf{z} \\ y \end{bmatrix} = \begin{bmatrix} -\dfrac{\partial g}{\partial \boldsymbol{\Phi}_j} \\ -\dfrac{\partial g}{\partial \lambda_j} \end{bmatrix} \tag{10}$$

The total design variation of the Lagrangian function, Eq. (7) gives

$$\frac{\mathrm{d}L}{\mathrm{d}b_i} = \frac{\mathrm{d}g}{\mathrm{d}b_i} + \left(\frac{\mathrm{d}\mathbf{z}}{\mathrm{d}b_i}\right)^{\mathrm{T}}(\mathbf{K}-\lambda_j\mathbf{M})\boldsymbol{\Phi}_j + \left(\frac{\mathrm{d}y}{\mathrm{d}b_i}\right)\left(\frac{1}{2} - \frac{1}{2}\boldsymbol{\Phi}_j^{\mathrm{T}}\mathbf{M}\boldsymbol{\Phi}_j\right) + \mathbf{z}^{\mathrm{T}}\frac{\mathrm{d}}{\mathrm{d}b_i}\{(\mathbf{K}-\lambda_j\mathbf{M})\boldsymbol{\Phi}_j\} + y\frac{\mathrm{d}}{\mathrm{d}b_i}\left\{\left(\frac{1}{2} - \frac{1}{2}\boldsymbol{\Phi}_j^{\mathrm{T}}\mathbf{M}\boldsymbol{\Phi}_j\right)\right\} \tag{11}$$

If $\mathbf{z}$ and y are selected to be in the same kinematically admissible space of $\boldsymbol{\Phi}_j$ and λ_j, the second and third terms of Eq. (11) vanish: i.e.

$$\left(\frac{\mathrm{d}\mathbf{z}}{\mathrm{d}b_i}\right)^{\mathrm{T}}(\mathbf{K}-\lambda_j\mathbf{M})\boldsymbol{\Phi}_j = 0$$
$$\left(\frac{\mathrm{d}y}{\mathrm{d}b_i}\right)\left(\frac{1}{2} - \frac{1}{2}\boldsymbol{\Phi}_j^{\mathrm{T}}\mathbf{M}\boldsymbol{\Phi}_j\right) = 0 \tag{12}$$

Then, Eq. (11) becomes

$$\frac{\mathrm{d}L}{\mathrm{d}b_i} = \frac{\partial g}{\partial b_i} + \mathbf{z}^{\mathrm{T}}\left(\frac{\mathrm{d}\mathbf{K}}{\mathrm{d}b_i} - \lambda_j\frac{\mathrm{d}\mathbf{M}}{\mathrm{d}b_i}\right)\boldsymbol{\Phi}_j - \frac{1}{2}y\boldsymbol{\Phi}_j^{\mathrm{T}}\frac{\mathrm{d}\mathbf{M}}{\mathrm{d}b_i}\boldsymbol{\Phi}_j + \frac{\mathrm{d}\lambda_j}{\mathrm{d}b_i}\left(\frac{\partial g}{\partial \lambda_j} - (\mathbf{z}^{\mathrm{T}}\mathbf{M}\boldsymbol{\Phi}_j)\right) + \frac{\mathrm{d}\boldsymbol{\Phi}_j}{\mathrm{d}b_i}\left(\frac{\partial g}{\partial \boldsymbol{\Phi}_j} + \mathbf{z}^{\mathrm{T}}(\mathbf{K}-\lambda_j\mathbf{M}) - y\boldsymbol{\Phi}_j^{\mathrm{T}}\mathbf{M}\right) \tag{13}$$

By using Eq. (8), we simplify Eq. (13) as

$$\frac{\mathrm{d}L}{\mathrm{d}b_i} = \frac{\partial g}{\partial b_i} + \mathbf{z}^{\mathrm{T}}\left(\frac{\mathrm{d}\mathbf{K}}{\mathrm{d}b_i} - \lambda_j\frac{\mathrm{d}\mathbf{M}}{\mathrm{d}b_i}\right)\boldsymbol{\Phi}_j - \frac{1}{2}y\boldsymbol{\Phi}_j^{\mathrm{T}}\frac{\mathrm{d}\mathbf{M}}{\mathrm{d}b_i}\boldsymbol{\Phi}_j \tag{14}$$

In addition, from the fundamental variational principle [21],

$$\frac{\mathrm{d}L}{\mathrm{d}b_i} = \frac{\mathrm{d}g}{\mathrm{d}b_i} \tag{15}$$

In this paper,

$$g = E_j = \sum_{i=1}^{n_n}(\mathbf{n}_i^{\mathrm{T}}\mathbf{N}\mathbf{T}_i\boldsymbol{\Phi}_j)^2 \tag{16}$$

Because the design variable, b_i, is the thickness of each element, t_e, Eq. (14) becomes:

$$\frac{\mathrm{d}E_j}{\mathrm{d}t_e} = \mathbf{z}^{\mathrm{T}}\left(\frac{\partial \mathbf{K}}{\partial t_e} - \lambda_j\frac{\partial \mathbf{M}}{\partial t_e}\right)\boldsymbol{\Phi}_j - \frac{1}{2}y\boldsymbol{\Phi}_j^{\mathrm{T}}\frac{\partial \mathbf{M}}{\partial t_e}\boldsymbol{\Phi}_j$$
$$= \mathbf{z}_e^{\mathrm{T}}\left(\frac{\partial \mathbf{k}_e(t_e)}{\partial t_e} - \lambda_j\frac{\partial \mathbf{m}_e(t_e)}{\partial t_e}\right)\boldsymbol{\Phi}_j^e - \frac{1}{2}y(\boldsymbol{\Phi}_j^e)^{\mathrm{T}}\frac{\partial \mathbf{m}_e(t_e)}{\partial t_e}\boldsymbol{\Phi}_j^e \tag{17}$$

where t_e is the thickness of the eth element and $\mathbf{k}_e$, $\mathbf{m}_e$ and $\boldsymbol{\Phi}_j^e$ are the element-wise stiffness matrix, mass matrix and eigenvector, respectively.

In order to calculate Eq. (17), we first obtain $\mathbf{z}_e$ and y by solving the adjoint equation, Eq. (10). By careful manipulation (see Appendix A for more detailed information), Eq. (10) becomes:

$$\begin{bmatrix} \mathbf{K}-\lambda_j\mathbf{M} & -\mathbf{M}\boldsymbol{\Phi}_j \\ -\boldsymbol{\Phi}_j^{\mathrm{T}}\mathbf{M} & 0 \end{bmatrix} \begin{bmatrix} \mathbf{z} \\ y \end{bmatrix} = \begin{bmatrix} -2\sum_{i=1}^{n_n}\left\{(\mathbf{n}_i^{\mathrm{T}}\mathbf{N}\mathbf{T}_i\boldsymbol{\Phi}_j)(\mathbf{N}\mathbf{T}_i)^{\mathrm{T}}\mathbf{n}_i\right\} \\ 0 \end{bmatrix} \tag{18}$$

for $\mathbf{z}$ and y.

The next step is to calculate $\partial \mathbf{k}_e(t_e)/\partial t_e$ and $\partial \mathbf{m}_e(t_e)/\partial t_e$. As expressed in Eq. (17), the stiffness and mass matrices of each element depend on only one design variable (in this paper, element thickness) that is associated with the given element. Therefore, the derivative of a response function can be transformed element wise. The problem is, however, that the shape functions of the shell elements in ANSYS are not open to the general public. This prohibits the development of any kind of analytic methods for obtaining sensitivity values. A simple alternative is to perturb one design variable at a time and then use a finite difference method (FDM) to approximate element stiffness matrix derivatives. If the number of design variables is large (712 in this case), this approach becomes very time consuming. In this paper, instead of using FDM, a regression model for the stiffness matrix was derived before performing the optimization procedure. Because the stiffness matrix depends only on the thickness of a shell element, the derivative of the local stiffness matrix can be approximated as follows:

$$\mathbf{k}_e(t_e) \cong \begin{bmatrix} \alpha_{11}t_e^3+\beta_{11}t_e^2+\gamma_{11}t_e+\delta_{11} & \alpha_{12}t_e^3+\beta_{12}t_e^2+\gamma_{12}t_e+\delta_{12} & \cdots & \alpha_{1n}t_e^3+\beta_{1n}t_e^2+\gamma_{1n}t_e+\delta_{1n} \\ \alpha_{21}t_e^3+\beta_{21}t_e^2+\gamma_{21}t_e+\delta_{21} & \alpha_{22}t_e^3+\beta_{22}t_e^2+\gamma_{22}t_e+\delta_{22} & \cdots & \alpha_{2n}t_e^3+\beta_{2n}t_e^2+\gamma_{2n}t_e+\delta_{2n} \\ \vdots & \vdots & \ddots & \vdots \\ \alpha_{n1}t_e^3+\beta_{n1}t_e^2+\gamma_{n1}t_e+\delta_{n1} & \alpha_{n2}t_e^3+\beta_{n2}t_e^2+\gamma_{n2}t_e+\delta_{n2} & \cdots & \alpha_{nn}t_e^3+\beta_{nn}t_e^2+\gamma_{nn}t_e+\delta_{nn} \end{bmatrix} \tag{19}$$

Therefore,

$$\frac{\partial \mathbf{k}_e(t_e)}{\partial t_e} \cong \begin{bmatrix} 3\alpha_{11}t_e^2+2\beta_{11}t_e+\gamma_{11} & 3\alpha_{12}t_e^2+2\beta_{12}t_e+\gamma_{12} & \cdots & 3\alpha_{1n}t_e^2+2\beta_{1n}t_e+\gamma_{1n} \\ 3\alpha_{21}t_e^2+2\beta_{21}t_e+\gamma_{21} & 3\alpha_{22}t_e^2+2\beta_{22}t_e+\gamma_{22} & \cdots & 3\alpha_{2n}t_e^2+2\beta_{2n}t_e+\gamma_{2n} \\ \vdots & \vdots & \ddots & \vdots \\ 3\alpha_{n1}t_e^2+2\beta_{n1}t_e+\gamma_{n1} & 3\alpha_{n2}t_e^2+2\beta_{n2}t_e+\gamma_{n2} & \cdots & 3\alpha_{nn}t_e^2+2\beta_{nn}t_e+\gamma_{nn} \end{bmatrix} \tag{20}$$

The general procedure of approximating a stiffness matrix is as follows:

1. Perform three structural analyses at the thickness cases of $(\frac{1}{3}t_0, \frac{2}{3}t_0, t_0)$.
2. Extract the stiffness components for the element from ANSYS for the three cases.
3. Using three data points for each component from Step 2, calculate α_{ij}, β_{ij} and γ_{ij} in Eq. (19) (because $\mathbf{k}_e(0)=\mathbf{0}, \delta_{ij}=0$ $\forall i$ and j).
4. Calculate $\partial \mathbf{k}_e(t_e)/\partial t_e$ from Eq. (20).

For the validation, we compared the sensitivity values from the proposed method with values from the FDM (Table 1). It is clearly shown that the design sensitivity analysis using the regressed stiffness matrix provides accurate results with an acceptable margin of error. The FDM results were obtained by using a perturbation of 1% and 0.1%.

2.3. Mode tracking

As the structural configuration changes at each iteration of optimization, "mode switching" may occur. If a certain objective or the constraint function is defined based on a fixed modal order, the corresponding sensitivities may be discontinuous at the time of mode switching, and an incorrect natural frequency and eigenmode may be obtained at the end of optimization. In order to keep tracking the target mode, a mode assurance criterion (MAC) [22] was utilized in this paper. The definition of MAC is as follows:

$$\mathbf{MAC}(\mathbf{\Phi}_a, \mathbf{\Phi}_b) = \frac{(\mathbf{\Phi}_a^{\mathrm{T}}\mathbf{\Phi}_b)^2}{(\mathbf{\Phi}_a^{\mathrm{T}}\mathbf{\Phi}_a)(\mathbf{\Phi}_b^{\mathrm{T}}\mathbf{\Phi}_b)} \tag{21}$$

where $\mathbf{\Phi}_a$ and $\mathbf{\Phi}_b$ represent two mode shape vectors of interest. The value of MAC varies between 0 and 1. When the MAC value is equal to 1, the two vectors represent exactly the same mode shape. We examined the norm of each extracted mode

Table 1
Accuracy of design sensitivity analysis using a regressed stiffness matrix.

Element	DSA with regression	FDM with 0.1% perturbation	FDM with 1% perturbation	Accuracy (%)
1	−2.13654	−2.13929	−2.11716	99.966
2	−3.21004	−3.22160	−3.19139	99.727
3	−3.18211	−3.17386	−3.14365	100.348
4	−1.78475	−1.78300	−1.76550	100.189
5	−4.18494	−4.17134	−4.13250	100.411
6	−6.61441	−6.63268	−6.56786	99.814
7	−7.14258	−7.13726	−7.06684	100.165
8	−5.03379	−5.03783	−4.98764	100.011
9	−7.41274	−7.41031	−7.33278	100.129
10	−6.81555	−6.82178	−6.75028	100.005

of the updated structural configuration with respect to the reference mode. At each iteration, the eigenvectors were compared with the old eigenvectors at the previous iteration, and then the eigenvector with the MAC value closest to 1 with respect to the reference eigenvector $\mathbf{\Phi}_{\text{ref}}$ was selected as the objective mode $\mathbf{\Phi}_{\text{obj}}$. This may be stated as follows:

$$\mathbf{\Phi}_{\text{obj}} = \mathbf{\Phi}_k \text{ such that } \max_{k=1..Nm} [\mathbf{MAC}(\mathbf{\Phi}_k, \mathbf{\Phi}_{\text{ref}})] \tag{22}$$

where N_m is the number of modes to be checked.

2.4. Procedure of nodal line optimization

Fig. 2 outlines the optimization procedure. A seamless integration between finite element analysis (FEA), design sensitivity analysis, and optimization module is crucial in an automated design process. ANSYS [23] is used for modal FEA and methods of moving asymptotes (MMA) [24] is employed to support design optimization with the subroutines of the design sensitivity modules coded in MATLAB [25].

2.5. Problem definition of nodal line optimization

As mentioned in Section 1, mode shapes (or the shape of nodal lines) and eigenfrequencies significantly affect sound parameters [1,2]. In the literatures [5,26], the second and fifth eigenmodes are generally selected for guidance in tuning because the two eigenmodes are sensitive to the thickness distributions and can be easily measured. In consideration of this fact, the objective function of nodal line optimization in this paper is to minimize the square sum of the displacement of selected nodes along the target nodal lines for the second (bending mode) and fifth (ring mode) eigenmodes. We also constrain eigenfrequencies within specific bandwidths. The optimization formulation including the constraints is as follows:

$$\begin{aligned} &\text{Minimize } \alpha \sum_{i=1}^{n_n} (w_2(\mathbf{x}_i))^2 + (1-\alpha) \sum_{i=1}^{n_n} (w_5(\mathbf{x}_i))^2 \\ &170\,(\text{Hz}) \le \lambda_2 \le 230\,(\text{Hz}) \\ &370\,(\text{Hz}) \le \lambda_5 \le 430\,(\text{Hz}) \\ &1.5\,(\text{mm}) \le t_m \le 5.0\,(\text{mm}), \quad m = 1,2,\ldots,n_e \end{aligned} \tag{23}$$

where α is a weighting factor (0.5 in this paper), and the initial values of t_m are uniformly set as 2.5 mm.

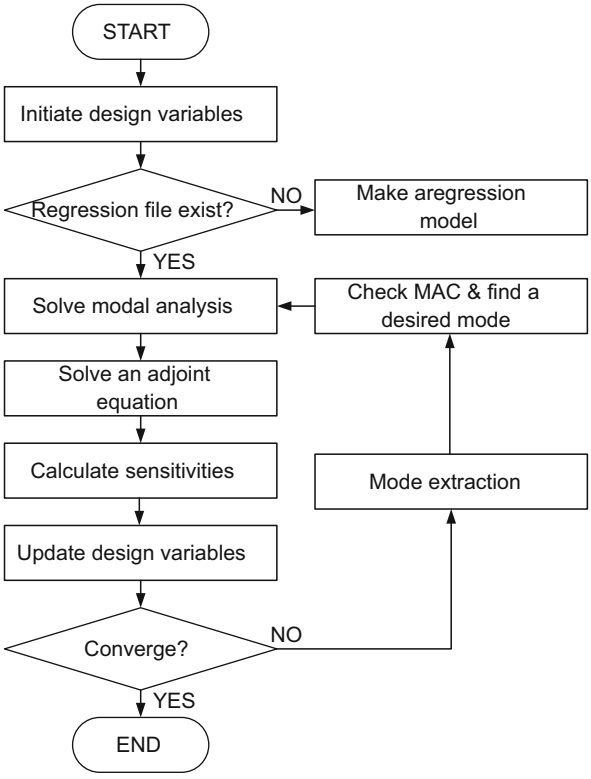

Fig. 2. Flow chart of nodal line optimization.

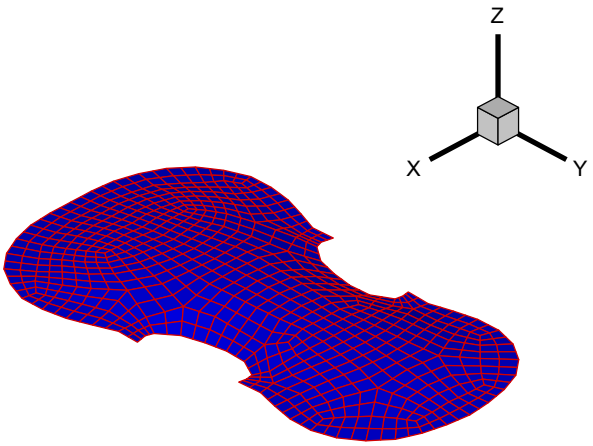

Fig. 3. Finite element model of a violin top plate.

Table 2
Material properties of a violin top plate.

Property	Value
E_{xx}	700 (kPa)
E_{yy}	16,000 (kPa)
E_{zz}	700 (kPa)
G_{xy}	900 (kPa)
G_{xz}	60 (kPa)
G_{xz}	900 (kPa)
μ_{xy}	0.02
μ_{xz}	0.47
μ_{yz}	0.42
ρ	0.4 (kg m^{-3})

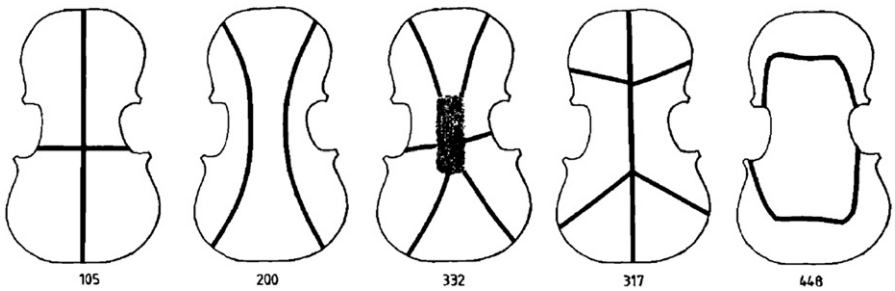

Fig. 4. Experimentally determined nodal lines and eigenfrequencies for modes 1–5 [3].

Fig. 3 shows a three-dimensional FE model of the violin top plate with a total of 712 finite elements, which are SHELL63 in ANSYS. Note that f-holes and a bass bar are not included in the FE model. We constructed the FE model based on the measurement of the coordinates of a violin top plate. The template violin top plate is made of spruce, which is highly anisotropic (Table 2). Because the shape functions of SHELL63 are not reported in the ANSYS user manual, we used a semi-analytic method to calculate sensitivity values: for the sensitivity derivation of eigenvalues, eigenvectors, stiffness and mass matrices, we used results from ANSYS.

3. Numerical results

Molin et al. [3] experimentally measured the nodal lines and eigenfrequencies of a violin top plate without f-holes and a bass bar from the first mode to the fifth mode as shown in Fig. 4.

In this paper, we numerically investigated nodal lines from the optimization by changing the weighting factor, α, in Eq. (23): 1 (only the second mode), 0 (only the fifth mode), and 0.5 (both the second and fifth modes). First, in the case of α=1 (Fig. 5(b)), the overall results are similar to Fig. 4 except a certain offset of the fifth mode from the desired shape.

Nodal lines with α=0 similarly deviated from the targeted nodal lines in the third and fourth modes (Fig. 5(c)). However, the value of 0.5 for α determined the desired nodal lines as shown in Fig. 5(d) by considering the second and fifth modes at the same time in Eq. (23). It is interesting to note that although a mode switch happened between the third and fourth modes during optimization we successfully obtained numerical results by tracking target modes as described in Section 2.3. Based on this finding, we used α=0.5 for the remaining numerical studies in the paper.

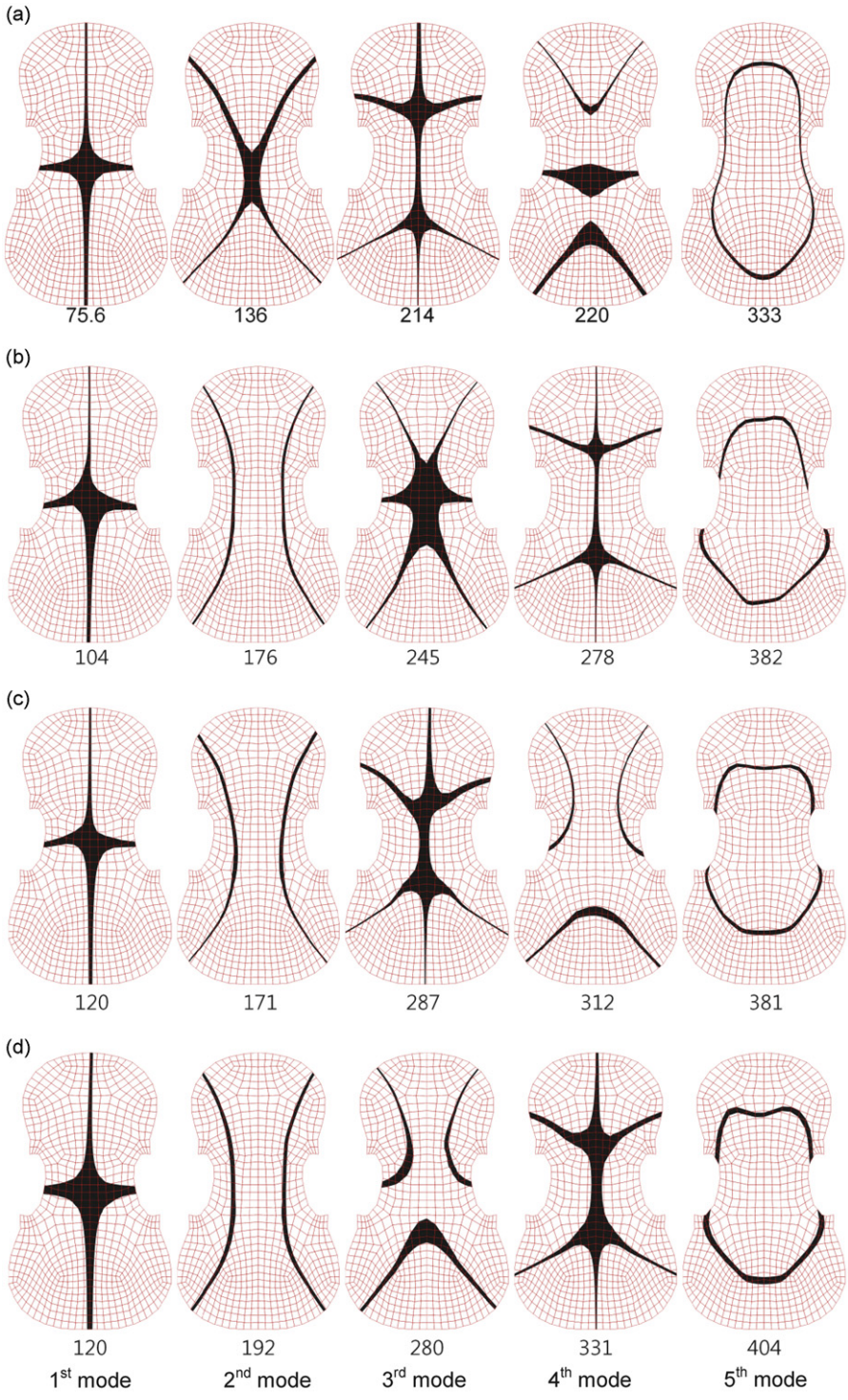

Fig. 5. Initial and optimized nodal lines of the first to the fifth modes: (a) Initial nodal lines; (b) optimized nodal lines in the case of α=1; (c) optimized nodal lines in the case of α=0 and (d) optimized nodal lines in the case of α=0.5.

We then checked target nodes and nodal lines for the second and fifth modes in the initial and optimized top plates. The initial top plate in which thickness distribution is uniform shows different nodal lines and eigenfrequencies from those desired. As shown in Fig. 6, however, the initial nodal lines for the second and fifth modes changed close to the targeted nodal lines as a result of minimization of the square sum of displacement of the target nodes. Ideally, optimization enables us to obtain both $E_2=0$ and $E_5=0$ in Eq. (5) (thus, $E=0.5E_2+0.5E_5=0$) by crossing all the target nodes, but we could not achieve this under the given FE model and constraint functions. Fig. 7 shows optimization histories of the objective function values and natural frequencies for the second and fifth modes.

Fig. 8 shows the general trend of thickness distribution of the optimized violin top plate. Starting from the uniform thickness, the thickness of the plate thicknesses was varied until the objective function was minimized and the constraint functions were satisfied. However, the thickness distribution obtained from optimization is inevitably discontinuous compared with the real top plate design.

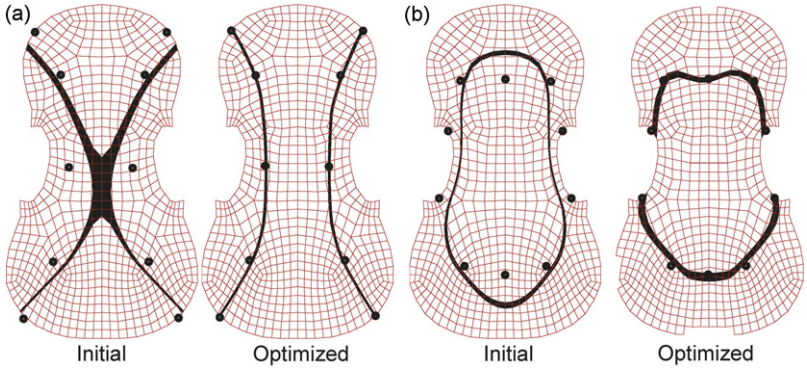

Fig. 6. Initial and optimized nodal lines: (a) second mode and (b) fifth mode.

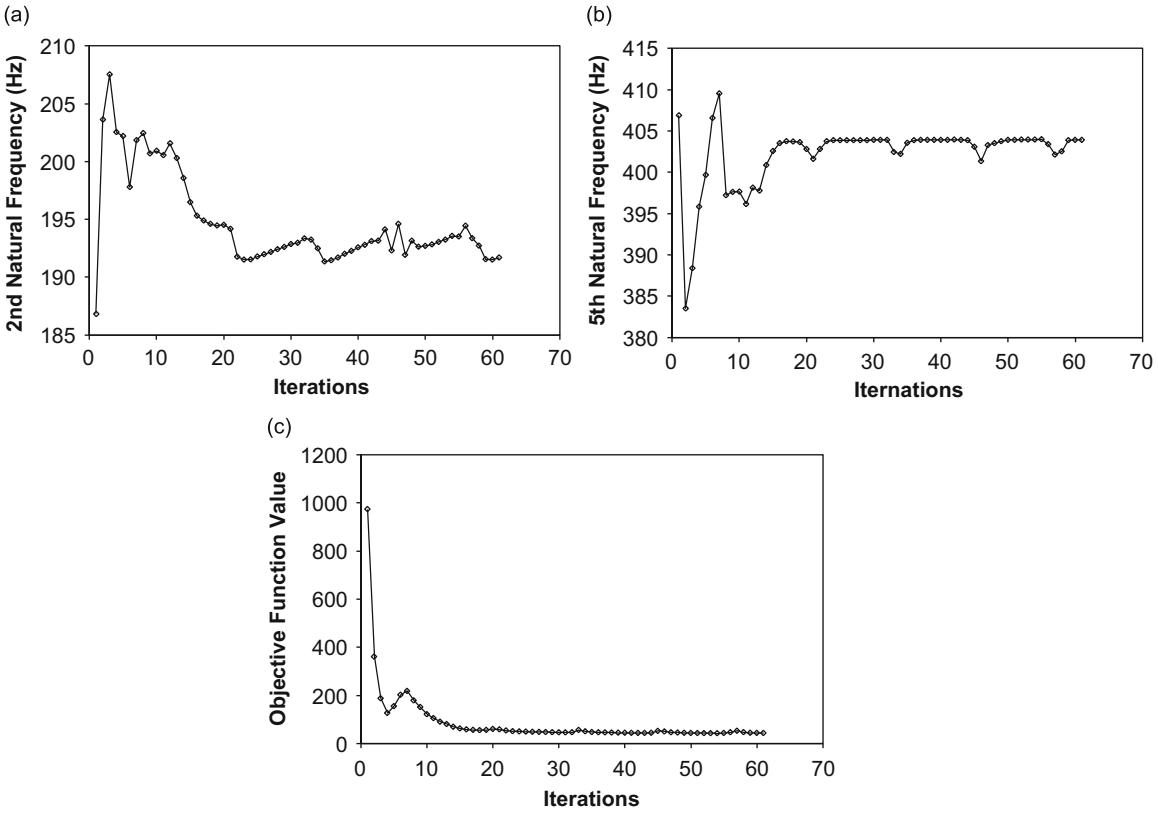

Fig. 7. Optimization histories of objective function values and the second and the fifth natural frequencies: (a) Second natural frequency; (b) fifth natural frequency and (c) objective function value.

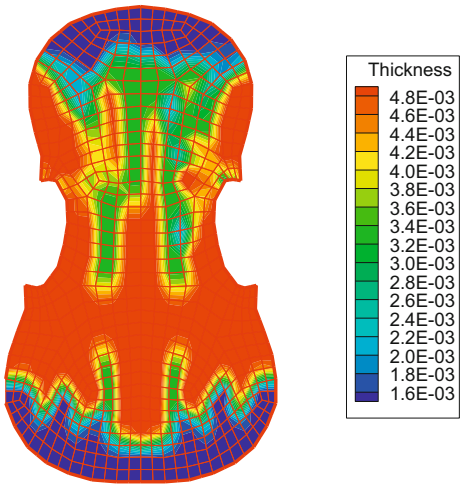

Fig. 8. Thickness distribution of the optimized violin top plate.

4. Conclusion

In this paper, we studied nodal line optimization for a violin top plate, a topic not previously considered in the field. For this purpose, we first proposed the concept of nodal line optimization, which minimizes the square sum of the displacement of target nodes located along the target nodal lines by varying the distribution of material thickness in a top plate. Next, we derived the sensitivities of the objective and constraint functions, which are essential for nodal line optimization, based on the approximation of the mass and stiffness matrices of a violin top plate. We then obtained numerical results and compared them with the experimental data in the literature for validation. The numerical framework for nodal line optimization proposed in this paper performed well to obtain targeted nodal lines within specific bandwidths of eigenfrequencies. From the viewpoint of manufacturability, however, the optimized thickness distribution which is discontinuous is not satisfactory. In further research, we may adopt numerical techniques to smooth out the discontinuous result or to obtain continuous distribution from the start. Considering other geometry variation (arching) and material properties (density and stiffness) as design variables would be also an interesting subject for the future work.

Acknowledgements

This research is partially supported by the Samsung Chair Endowment fund. The authors would like to thank Dr. Krister Svanberg at KTH (Stockholm, Sweden) for providing the MMA code for academic research.

Appendix A. Matrix calculus notation [19,27]

Let $\mathbf{x}$ be a k vector of real variables, $\mathbf{y}$ be an m vector of real variables, $a(\mathbf{x},\mathbf{y})$ be a scalar differentiable function of $\mathbf{x}$ and $\mathbf{y}$, and $\mathbf{g}(\mathbf{x},\mathbf{y}) = [\,g_1(\mathbf{x},\mathbf{y}) \quad \cdots \quad g_n(\mathbf{x},\mathbf{y})\,]^{\mathrm{T}}$ be an n vector of differentiable functions of $\mathbf{x}$ and y. Using i as row index and j as column index, define

$$a_{\boldsymbol{x}} \equiv \frac{\partial a}{\partial \mathbf{x}} \equiv \left[\frac{\partial a}{\partial x_j}\right]_{1\times k} \tag{A.1}$$

$$\mathbf{g}_x \equiv \frac{\partial \mathbf{g}}{\partial \mathbf{x}} \equiv \left[\frac{\partial \mathbf{g}}{\partial x_j}\right]_{n\times k} \tag{A.2}$$

$$a_{xy} \equiv \left[\frac{\partial^2 a}{\partial x_i \partial y_j}\right]_{k\times m} = \frac{\partial}{\partial \mathbf{y}}\left[\frac{\partial a^{\mathrm{T}}}{\partial \mathbf{x}}\right] = \frac{\partial}{\partial \mathbf{y}}\left[a_x^{\mathrm{T}}\right] = \left[a_x^{\mathrm{T}}\right]_y \tag{A.3}$$

Note that the derivative of a scalar function with respect to a vector variable in Eq. (A.1) gives a row vector. In order to take advantage of this notation, it is important that the correct vector definition of matrix derivatives be used. Note also that the derivative of a vector function with respect to a vector variable in Eq. (A.2) gives a matrix.

Based on the above notation, matrix calculus extensions of ordinary calculus rules can be derived. For example, if $\mathbf{A}$ is an $n \times n$ constant matrix,

$$\begin{aligned}\frac{\partial}{\partial \mathbf{x}}(\mathbf{A}\mathbf{g}(\mathbf{x},\mathbf{y})) &= \left[\frac{\partial}{\partial x_j}\left(\sum_{l=1}^{n} A_{il} g_l\right)\right] \\ &= \left[\left(\sum_{l=1}^{n} A_{il}\frac{\partial g_l}{\partial x_i}\right)\right] \\ &= \mathbf{A}\frac{\partial \mathbf{g}}{\partial \mathbf{x}} = \mathbf{A}\mathbf{g}_x \end{aligned} \tag{A.4}$$

The second example involves two n-vector functions $\mathbf{h}(\mathbf{x},\mathbf{y})$and $\mathbf{g}(\mathbf{x},\mathbf{y})$. By careful manipulation,

$$\begin{aligned}\frac{\partial}{\partial \mathbf{x}}(\mathbf{g}^{\mathrm{T}}\mathbf{h}) &= \left[\frac{\partial}{\partial x_j}\left(\sum_{l=1}^{n} g_l h_l\right)\right] \\ &= \left[\sum_{l=1}^{n}\left(\frac{\partial g_l}{\partial x_j}h_l + g_l\frac{\partial h_l}{\partial x_j}\right)\right] \\ &= \left[\sum_{l=1}^{n} h_l\frac{\partial g_l}{\partial x_j}\right] + \left[\sum_{l=1}^{n} g_l\frac{\partial h_l}{\partial x_j}\right] \\ &= \mathbf{h}^{\mathrm{T}}\frac{\partial \mathbf{g}}{\partial \mathbf{x}} + \mathbf{g}^{\mathrm{T}}\frac{\partial \mathbf{g}}{\partial \mathbf{x}} \\ &= \mathbf{h}^{\mathrm{T}}\mathbf{g}_x + \mathbf{g}^{\mathrm{T}}\mathbf{h}_x \end{aligned} \tag{A.5}$$

Very often in structural mechanics, quadratic forms $\mathbf{x}^{\mathrm{T}}\mathbf{A}\mathbf{x}$ $(\mathbf{x} \in R^n)$ arise, where $\mathbf{A}$ is a $n \times n$ constant matrix, presumed initially not to be symmetric. Using the foregoing definitions,

$$\begin{aligned}\frac{\partial}{\partial \mathbf{x}}(\mathbf{x}^{\mathrm{T}}\mathbf{A}\mathbf{x}) &= \left[\frac{\partial}{\partial x_i}\left(\sum_{j,k}^{n} x_k a_{kj} x_j\right)\right] \\ &= \left[\sum_{k}^{n} x_k a_{ki} + \sum_{j}^{n} a_{ij} x_j\right] \\ &= \left[\sum_{k}^{n} x_k a_{ki} + \sum_{j}^{n} x_j a_{ji}^{\mathrm{T}}\right] \\ &= \mathbf{x}^{\mathrm{T}}(\mathbf{A} + \mathbf{A}^{\mathrm{T}}) \end{aligned} \tag{A.6}$$

In particular, if $\mathbf{A}$ is symmetric,

$$\frac{\partial}{\partial \mathbf{x}}(\mathbf{x}^{\mathrm{T}}\mathbf{A}\mathbf{x}) = 2\mathbf{x}^{\mathrm{T}}\mathbf{A} \tag{A.7}$$

References

[1] C.M. Hutchins, V. Benade, *Research Papers in Violin Acoustics 1975–1993*, Acoustical Society of America, 1997.
[2] E.V. Jansson, J.A. Moral, J. Niewczyk, Experiments with free violin plates, *Journal of Catgut Acoustical Society* 1 (2) (1988) 2–6.
[3] N.E. Molin, L.E. Lindgren, E.V. Jansson, Parameters of violin plates and their influence of the plate modes, *Journal of Catgut Acoustical Society* 83 (1) (1987) 281–291.
[4] O.E. Rodgers, Influence of local thickness changes on violin plate frequencies, *Journal of Catgut Acoustical Society* 1 (1990) 6–10.
[5] E. Jansson, *Acoustics for Violin and Guitar Makers*, Kungl. Tekniska hogskolan, Department of Speech, Music and Hearing, 2002.
[6] R.J. Yang, Multidiscipline topology optimization, *Computer & Structure* 63 (1997) 1205–1212.
[7] A.R. Diaz, N. Kikuchi, Solutions to shape and topology eigenvalue optimization problems using a homogenization method, *International Journal for Numerical Methods in Engineering* 35 (2005) 1487–1502.
[8] M. Tinnsten, P. Carlsson, Numerical optimization of violin top plates, *Acustica United with Acta Acustica* 88 (2) (2002) 278–285.
[9] P. Carlsson, M. Tinnsten, A distributed computing system used for concurrent optimization methods on a violin top, *Structural and Multidisciplinary Optimization* 25 (5) (2003) 453–458.
[10] J.I. Pritchard, H.M. Adelman, R.T. Haftka, Sensitivity analysis and optimization of nodal point placement for vibration reduction, *Journal of Sound and Vibration* 119 (1987) 277–289.
[11] E. Lai, G.K. Ananthasuresh, On the design of bars and beams for desired mode shapes, *Journal of Sound and Vibration* 254 (2002) 393–406.
[12] A.R. Inzarulfaisham, H. Azegami, Solution to boundary shape optimization problem of linear elastic continua with prescribed natural vibration mode shapes, *Structural Multidisciplinary Optimization* 27 (2004) 210–217.
[13] A.R. Inzarulfaisham, H. Azegami, Shape optimization of linear elastic continua for moving nodes of natural vibration mode to assigned positions and its application to chassis-like frame structures, *Transactions of the Japan Society for Computational Engineering and Science* 7 (2005) 43–50.
[14] M.P. Bendsøe, N. Kikuchi, Generating optimal topologies in structural design using a homogenization method, *Computer Methods in Applied Mechanics and Engineering* 71 (1988) 197–224.
[15] M.P. Bendsøe, Optimal shape design as a material distribution problem, *Structural Optimization* 1 (1989) 193–202.
[16] I.Y. Kim, B.M. Kwak, Design space optimization using a numerical design continuation method, *International Journal for Numerical Methods in Engineering* 53 (2002) 1979–2002.
[17] I.G. Jang, B.M. Kwak, Evolutionary topology optimization using design space adjustment based on fixed grid, *International Journal for Numerical Methods in Engineering* 66 (2006) 1817–1840.

[18] Y. Maeda, S. Nishiwaki, K. Izui, M. Yoshimura, K. Matsui, K. Terada, Structural topology optimization of vibrating structures with specified eigenfrequencies and eigenmode shapes, *International Journal for Numerical Methods in Engineering* 67 (2006) 597–628.
[19] K.K. Choi, N.H. Kim, *Structural Sensitivity Analysis and Optimization*, Springer, New York, 2004.
[20] T.H. Lee, Adjoint method for design sensitivity analysis of multiple eigenvalues and associated eigenvectors, *Journal of American Institute of Aeronautics and Astronautics* 45 (2007) 1998–2004.
[21] J.S. Arora, J.B. Cardoso, Variational principle for shape design sensitivity analysis, *Journal of American Institute of Aeronautics and Astronautics* 30 (1992) 538–547.
[22] T.S. Kim, Y.Y. Kim, Mac-based mode-tracking in structural topology optimization, *Computer & Structure* 74 (2000) 375–383.
[23] Theory Reference for ANSYS and ANSYS Workbench, ANSYS Inc., Canonsburg, United States, 2006.
[24] K. Svanberg, The method of moving asymptotes—a new method for structural optimization, *International Journal for Numerical Methods in Engineering* 24 (1987) 359–373.
[25] MATLAB 7.0.1 Optimization Toolbox 3 User's Guide, MathWorks Inc., Natick, United States, 2004.
[26] G. Bissinger, C. Hutchins, Tuning the bass bar in a violin plate, *Catgut Acoustical Society Newsletter* 26 (1976) 10–12.
[27] C. Goffman, *Calculus of Several Variables*, Harper & Row, New York, 1965.